

# RFSOI n-MOSFET OI-Layer Ground-Plane Engineering with Quasi-3D Simulations

Daniel Connelly<sup>†</sup>, Hiu Yung Wong<sup>\*</sup>, Richard Burton<sup>†</sup>, Hideki Takeuchi<sup>†</sup>, Robert Mears<sup>†</sup>  
 daniel.connelly@atomera.com, <sup>†</sup>Atomera Inc, <sup>\*</sup>San Jose State University

**Abstract**—Here we demonstrate a novel quasi-3D simulation technique for partially depleted RFSOI MOSFETs, modeling the use of oxygen-inserted (OI) layers to form a p+ ground plane in the SOI by immobilizing boron acceptors within the SOI layer. Using a custom process model, 2D “slice” device simulations along the device width, and post-processing for the electrostatic potential variation between slices, we show improved potential uniformity due to the 20% to 90% superior body conductance from the ground plane. Results agree with 3D simulations with a matched mesh, although the quasi-3D method allows for a finer mesh suitable for treating the steep doping gradients associated with the OI ground plane.

## I. INTRODUCTION

RFSOI MOSFETs [1] consist of source, drain, and gate contacts which extend over the full width of one or more “fingers” but with body contacts only at the edges. Body current must flow along the width axis to reach the channel center. These currents, either due to transient switching or quasi-static current between the body and the source or drain, cause an ohmic drop along the width, inducing body effects [2], rendering simple 2D simulations [3] insufficient. In contrast the source, drain, and gate potentials have a relatively constant potential due to lower resistance.

Thus while the device may have nanometer-scale detail in each cross-section along the width axis, potential variations along the width are typically over a micrometer scale. 3D modeling [4] may require an excessive number of mesh points to capture the detailed cross-section.

Our hybrid approach models cross-sections in 2D, coupling these solutions by solving body current and potential as a function of position along the width axis. This “gradual channel” approximation assumes current flowing along the width axis is essentially decoupled from current flowing in the perpendicular, “slice” plane. Each 2D slice is characterized by its own body potential, the body potential gradient determined by body current and body conductance. This is what we call a “quasi-3D method”.

This method allows for studying the advantage of ground-plane engineering using oxygen-inserted (OI) layers, which trap immobilize active dopants including boron and phosphorus by a combination of dopant and point-defect trapping [5-6].

## II. QUASI-3D METHOD

A first approximation is of quasi-equilibrium: each 2D slice is characterized by the hole quasi-Fermi level in the un-depleted body of the partially depleted SOI n-FET. This is a key assumption which should be tested against 3D simulations: current flowing perpendicular to a slice has no effect on the potential and charge distributions within the slice, for a given body potential, averaged over holes (n-FET) or electrons (p-FET) within the slice.

A second approximation is that current continuity can be quantified on a slice-by-slice basis, rather than locally. Net

current in each 2D section adds or subtracts from the net width-axis ( $z$ -axis) flux:

$$I_B(z) = \int_z^{W/2} dz' J_{B2D}(z') \quad (1)$$

where  $J_{B2D} dz$  is the hole current from the thin 2D slice, and total body current =  $2 I_B(z=0)$ , with contacts at each edge.

The  $z$ -dependence of  $J_{B2D}$  is unknown. However, 2D simulations can be used to determine its body potential dependence. Post-processing can then be used to match body potential to  $z$ .

The third approximation is that mobility-weighted hole concentrations (n-FET) can be integrated across the body cross-section to map body potentials to position. A “gradual channel” approximation is used:  $I_B(z)$ , where  $z$  goes from 0 at the edge to  $W/2$  mid-channel (symmetric with  $W$  to  $W/2$ ), is assumed to be proportional to the product of the gradient of the body potential and the net hole (n-FET) conductance:

$$I_B(z) = -q \iint dx dy p \mu_h \nabla_z \phi_h \approx -q \nabla_z \langle \phi_h \rangle \iint dx dy p \mu_h \quad (2)$$

where  $x, y$  are the coordinates in each slice,  $p$  is the hole concentration,  $\mu_h$  is a relevant hole mobility, and  $\langle \phi_h \rangle$  is the average hole quasi-Fermi potential (averaged over holes). Integrals are done over the body cross-section (excluding any artificial body-tie into the buried oxide). This equation allows for solving  $\langle \phi_h \rangle(z)$  (henceforth referred to as  $\phi_h(z)$ ) and  $I_B(z)$  via numerical integration.

A fourth approximation is that  $J_{B2D}$  flowing into a body tie in a 2D simulation matches the contribution per unit width of body current in a 3D simulation at the same local body potential, even though the current paths are different. This assumption relies on the hole quasi-Fermi potential being relatively constant in the cross-section.

For a given body contact bias and  $I_B(z=0)$ , we know  $\phi_h$  at the edge  $z=0$ , but to get the  $z$ -dependence:

1. Perform a 2D process simulation.
2. Create an artificial body tie (to the substrate or to a separate contact).
3. Start the body bias at slightly more negative than the 3D contact bias, to allow for quasi-Fermi gradients between the contact and the SOI.
4. Ramp up the body bias with sufficiently small steps, extracting  $\phi_h$ , body conductance (2),  $J_{S2D}$ ,  $J_{D2D}$ , and  $J_{B2D}$  to a “floating body” limit  $J_{B2D} = 0$ , or breakdown, whichever is first.
5. With post-processing, self-consistently map 2D simulations to  $z$ . Start at  $z=0$  with  $\phi_h = V_B - I_B R_X$ , where  $R_X$  is an extrinsic resistance. Using the ohmic drop from edge to center (2) and the accumulated base current from center to edge (1) for each required  $\phi_h$  value, interpolate conductance and current densities from the 2D results.

So start with a fixed  $I_B(z=0)$ , then integrate inward until that is depleted. Mid-channel for that  $I_B(z=0)$  is where local  $I_B(z)$  drops to zero. To solve for a specific width, the estimate

of  $I_B(0)$  is iterated until the  $I_B(z) = 0$  at the target  $z = W/2$ , if such a solution exists.

### III. TWO-DIMENSIONAL SIMULATION

#### A. Process Simulation

2D *S-Process* [7] simulations were done with control SOI n-FETs, SOI with oxygen inserted layer stacks (“OI”) 30 nm from the buried oxide, and SOI with an additional OI stack 30 nm from the top surface (“double OI”). OI layer kinetics were treated using a custom model consisting of differential equations implemented with the *Alagator* scripting language in *S-Process*.

Three boron doses were modeled. Fig. 1 shows long-channel boron profiles (control and OI cases) and 2D cross-sections (single and double OI layers). A deep OI stack forms a “ground plane” by immobilizing boron, while the shallower OI stack reduces dopant in the channel region.

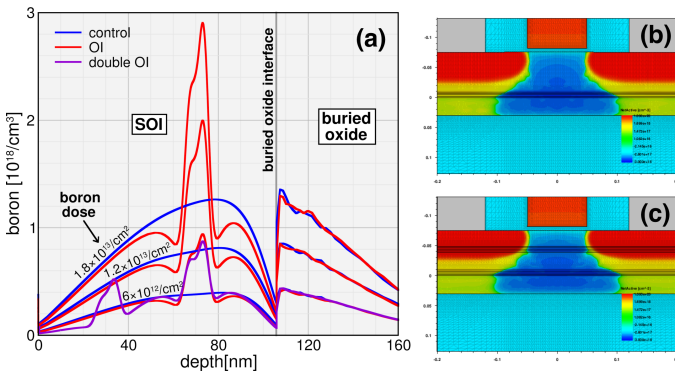


Fig. 1: (a) Simulated long-channel boron profiles for standard silicon epitaxy and for films with “OI” inserted oxygen layers. The OI causes a pile-up of active boron. (b) Cross-section with OI stack forming a ground plane. (c) Cross-section with double OI stack.

#### B. 2D Body Ties

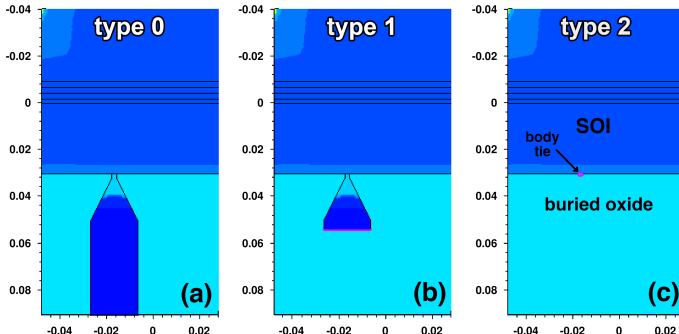


Fig. 2: Body tie options, with net doping contours in silicon (blue = p-type): (a) semiconductor to substrate, (b) semiconductor to buried well contact, (c) direct equilibrium Ohmic contact to SOI. Cross-sections show OI layers as horizontal lines.

Two-dimensional simulations require an artificial body tie. In our work three types were used, illustrated in Fig. 2:

- **type 0:** Drill a p+ slot through the buried oxide to the substrate, and bias the substrate to control body potential.
- **type 1:** Create a shallow p+ contact in the buried oxide, biased independently from the substrate.

- **type 2:** Make a direct “equilibrium Ohmic” contact to the bottom of the SOI layer, biased independently, which does not perturb the zero-bias solution.

In types 0-1 an e.g. 0.1 eV band offset was used to confine holes in the artificial contact regions. The p+ doping was tapered proximate to the SOI. Contact regions were assigned a high mobility to reduce potential drops. Contacts were placed 1/3 of the way between the source and drain, since the drain depletion region tends to extend further under the gate.

An example of applying a body tie to a control (no OI) FET is shown in Fig. 2. There was negligible effect on the hole distribution when the body potential was matched.

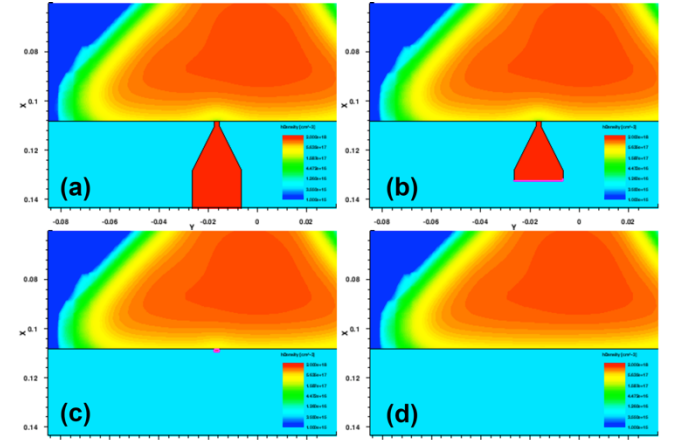


Fig. 3: Comparison of hole profiles with body contact schemes, with  $V_B = 0.12$  chosen to match the floating body case, and  $V_D = 1$  V,  $V_G = -1$  V, showing only small perturbations due to contacts: (a) type 0 p+ contact to substrate, (b) type 1 p+ contact in buried oxide, (c) type 2 equilibrium Ohmic contact directly to body, (d) floating body.

#### C. Device Simulation

2D *S-Device* [8] results are shown in Figs. 2-3. The body and gate were biased at  $-1$  V, the source at  $0$  V, and various drain biases were applied. The 2D substrate bias was ramped upward until either the magnitude of  $I_B$  increased dramatically, or reached zero (the floating body limit).

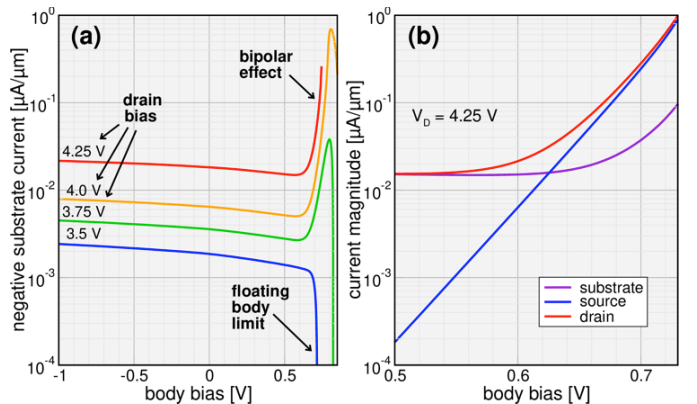


Fig. 2: 2D ramped  $V_B$  simulations: (a) body tie current  $J_{B2D}$  either goes positive as body-source becomes forward biased, or goes more negative due to bipolar effect [9,10] at higher  $V_D$ . (b) At  $V_D = 4.25$  V, body triggers bipolar action between the drain and source.

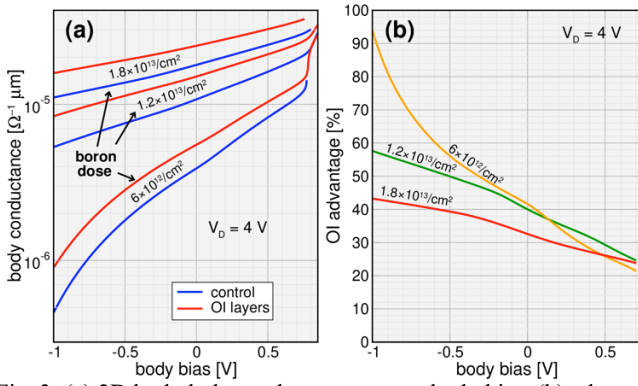


Fig. 3: (a) 2D body hole conductance versus body bias, (b) advantage from an OI layer stack ground-plane. A double OI stack is similar. OI layers result in a 40%-90% conductance increase, a 30%-50% lower resistance.

#### IV. THREE-DIMENSIONAL CALCULATION

After slices were simulated, the quasi-3D method was used to map  $\phi_h$  to  $z$ . The quasi-3D method was coded in *S-Visual* [11]. Fig. 4 shows  $\phi_h$  mapping to  $z$ , and  $I_B$  decreasing to zero mid-channel ( $z = W/2$ ). Full width was 100  $\mu\text{m}$ , unless there was no solution for the selected edge  $I_B$ . Then it was the maximum width (“snapback width”).

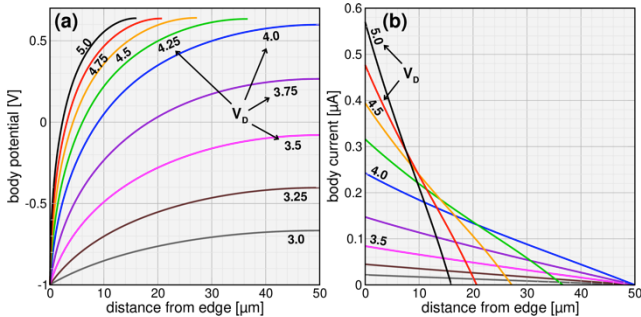


Fig. 4: Results versus  $z$ ,  $W = 100 \mu\text{m}$  ( $V_D \leq 4 \text{ V}$ ), or maximum value ( $V_D > 4 \text{ V}$ ). (a) Body potential increases from the nominal  $-1\text{ V}$  at the channel edge, moving inward to the mid-channel. (b)  $I_B(z)$  falls from the channel edge to zero mid-channel.

Fig. 5 shows the “width snap-back” effect. For widths near the limit supporting a chosen body current, there were two solutions, and for sufficiently higher currents, there was no solution. Ground plane engineering with OI layers increased this maximum width.

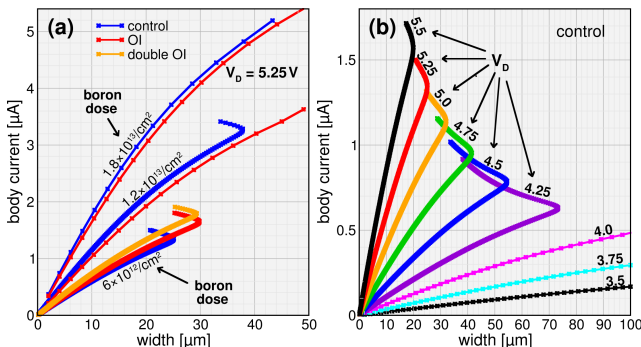


Fig. 5: Body current versus channel width. Note the “width snap-back” behavior. (a) Width snap-back was at larger  $W$  with OI. (b) Higher  $V_D$  reduced the snap-back width (control only shown).

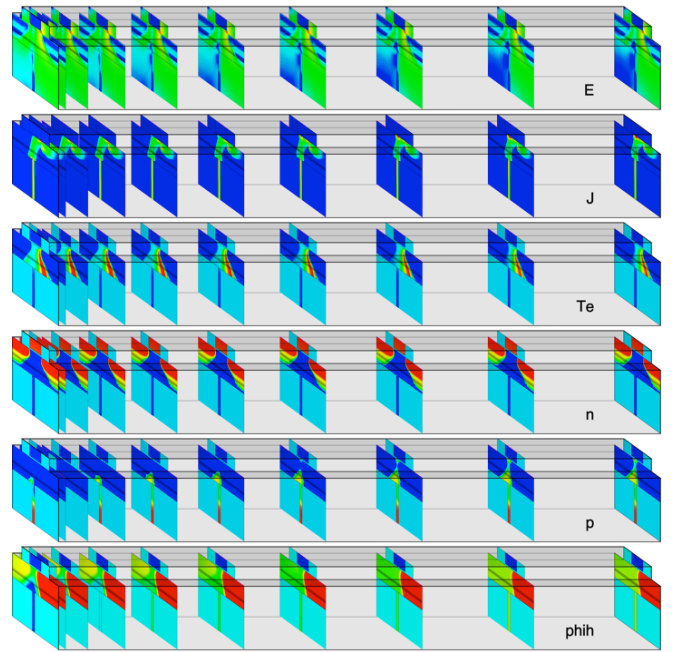


Fig. 6: Extrusion of 2D simulations along the width axis  $z$ , with the channel edge to the left, and mid-channel to the right. Slices were generated with a  $V_B$  ramp.  $V_B$  values were then mapped to position by solving (1) and (2) self-consistently.

Fig. 6 schematically illustrates the  $z$ -mapping of slices of uniform  $\phi_h$  spacing. Slices are more closely spaced to the left, where the potential gradient is steepest.

#### V. COMPARISON WITH 3D

3D simulations were performed to validate the primary assumptions of this method: that  $I_B(z)$  does not invalidate the 2D solutions, that the  $\phi_h$  gradient in (2) can be moved outside the integral, and that current collected by the 2D body ties can be used to calculate the 3D current flowing to the body edge. These simulations used simplified models and a coarser mesh due to the large 3D domain. The same mesh refinement criteria were used in 2D to match artifacts associated with the coarse mesh (see Figs. 7a-b).

To test the first assumption two device widths (10  $\mu\text{m}$  and 20  $\mu\text{m}$ ) were simulated, each with two values for bulk phonon scattering (Coulomb scattering was also used). For a given drain, source, and gate bias, slices were then taken along the width, and for each, the body potential was averaged over the hole population. The  $z$ -component of hole current was integrated over the SOI region of each slice.

The result is in Fig. 7d, where each split has its own curve of body current versus  $\phi_h$ . So if body current affects the solution of hole density, then the net hole concentration should also differ as a function of  $\phi_h$  for each of the four splits. But the curves in Fig. 7c overlap: body current does not significantly affect the holes. This supports the first assumption.

The body potential  $\phi_h$  (Fig. 7e) and body current (Fig. 7f) are plotted versus position next. The 2D and 3D results generally agree, supporting the approach of collecting current with a body tie in the 2D simulations, and assuming that same

current/width flows to the edge in the actual device. Note the 3D device (symbols) has a distributed body tie near the edge, explaining the rapid drop in current near  $z = 0$ .

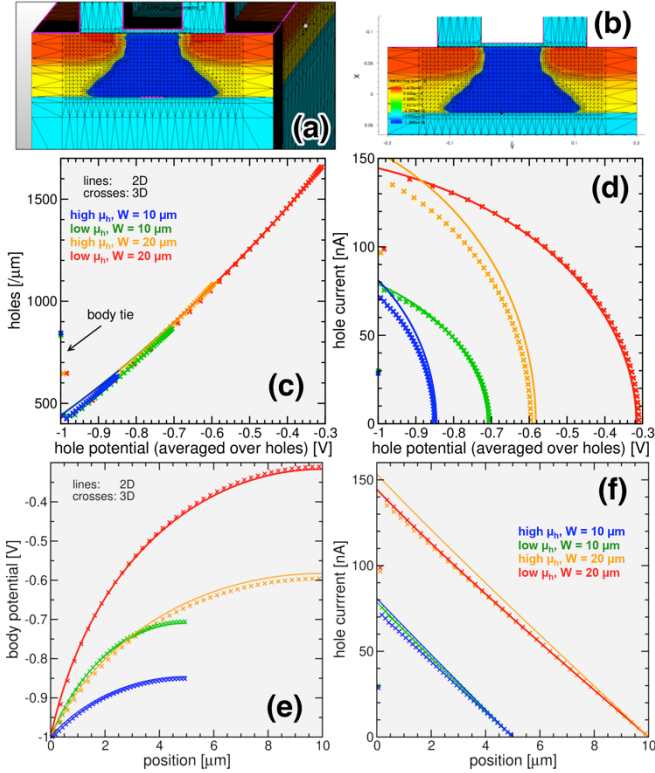


Fig. 7: 2D to 3D comparison: (a) 3D mesh. (b) 2D mesh, using same refinement criteria. (c) holes vs.  $\phi_h$ : curves coincide, so no  $I_B$  dependence. (d) body current  $I_B$  versus  $\phi_h$ :  $\mu_h$  and  $W$  affect  $I_B$ . (e)  $\phi_h$  versus  $z$ , showing match of 3D with quasi-3D. (f)  $I_B$  versus  $z$ .

## VI. MIXED MODE ALTERNATIVE

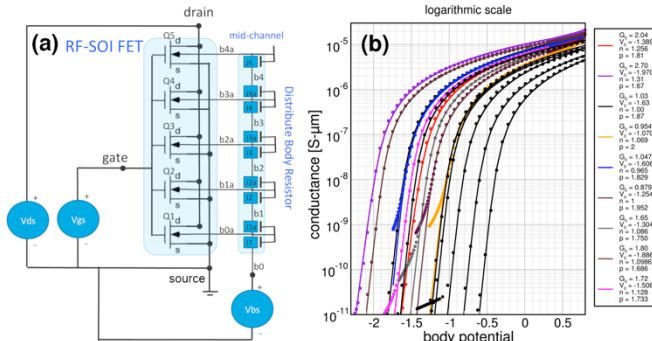


Fig. 8: (a) schematic of S-Device mixed-mode representation of wide RFSOI device. Slices are simulated in 2D, while distributed body resistance uses a compact model. (b) calibration of compact conductance model (lines) to 2D (points) for various biases. Fits are combined using voltage coefficients to yield the full model.

An alternate approach to this post-processing technique is to treat successive slices as TCAD circuit elements, connected with a compact model for the body conductance  $G_{body}$ . Here is a preliminary voltage controlled resistor model, with electrical resistance  $R = (\Delta z / G_{body})$ , where  $\Delta z$  is the slice separation:

$$G_{body} = G_0 \left( \frac{T_0}{T} \right)^a \left( \ln \left| 1 + e^{\frac{V_{eff} - V_p}{npk_B T}} \right| \right)^p, \quad (3)$$

where  $V_p$  is a function of  $T$ ,  $T_0 = 300K$ ,  $V_{eff}$  is a linear combination of node voltages, and  $a$ ,  $n$  and  $p$  are coefficients.

A schematic of the circuit is shown in Fig. 8a, with the partial calibration of a compact model shown in Fig. 8b.

This method allows for nodes (source, drain, gate, and body contact) to be independently ramped: the quasi-3D method uses a body bias ramp for each bias of the other terminals. A disadvantage is that body resistance is only approximately treated, via the calibrated compact model. Another is that the 2D simulations of the slices are calculated simultaneously and self-consistently with the circuit network, which increases the computational complexity, thus limiting the number of slices and/or mesh density. However, for ramping the drain bias, it may be the best approach, an intermediate level between the quasi-3D method and full 3D.

## VII. LIMITATIONS

The method relies on a continuous hole layer and gradually varying potentials calculated with low-field mobility. A 3D simulation of a pinched-off body is shown in Fig. 9. Generally any “3D” effects near the channel edge will not be directly captured.

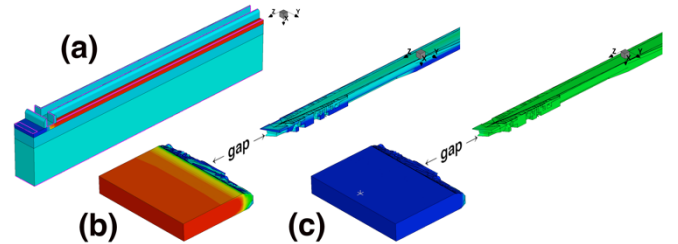


Fig. 9: 3D simulation example showing limitation of quasi-3D method. (a) 3D half-device. (b) Near edge, showing hole density, from  $10^{17}/\text{cm}^3$ , with lower concentrations transparent: contact is “pinched off” from the channel. (c)  $\phi_h$  jumps from  $-2.5$  V (contact), to  $-1.5$  V (channel) across the fully-depleted pinched-off region (gap).

## VIII. CONCLUSION

The quasi-3D method couples finely meshed 2D simulations, with ramped body potential, by mapping body potential to position along the width axis using a self-consistent solution of body current and body potential, using a body conductance extracted as a function of potential from the 2D simulations. The method compares well with full 3D simulation, but allows for finer meshing consistent with resolving detailed cross-sections such as those resulting from doping engineering with OI layers. The method allows the demonstration of reduced potential variation along the body width when creating a boron ground plane using OI layers formed in the SOI. An alternate approach, using a calibrated compact model for body resistance, can also be used in a mixed-mode simulation.

## IX. REFERENCES

- [1] R Wolf *et al.*, "A Thin-film SOI 180nm CMOS RF switch", SiRF 2009.
- [2] H. Lee, *et al.*, "Analysis of body bias effect with PD-SOI for analog and RF applications", *Solid-State Electronics*, **46**(8), 2002, pp. 1169-1176, [https://doi.org/10.1016/S0038-1101\(02\)00011-4](https://doi.org/10.1016/S0038-1101(02)00011-4).
- [3] H.W. Wei and H.S. Rusian, "Investigation of FDSOI and PDSOI MOSFET characteristics", *AIP Conference Proceedings* 2173, 020005 (2019); <https://doi.org/10.1063/1.5133920> Published Online: 11 November 2019.
- [4] A. Daghighi and M. A. Osman, "Three-dimensional simulation of body contact structures in PD SOI MOSFETs," *Proceedings of the 15th Biennial University/Government/ Industry Microelectronics Symposium (Cat. No.03CH37488)*, Boise, ID, USA, 2003, pp. 288-291, doi: 10.1109/UGIM.2003.1225745.
- [5] D. Connelly *et al.*, "Suppressing Oxidation-Enhanced Diffusion of Boron in Silicon With Oxygen-Inserted Layers," in *IEEE Journal of the Electron Devices Society*, vol. 6, pp. 1173-1178, 2018, doi: 10.1109/JEDS.2018.2872689.
- [6] X. Xiang, *et al.*, "Effects of oxygen-inserted layers on diffusion of boron, phosphorus, and arsenic in silicon for ultra-shallow junction formation", *Journal of Applied Physics* 123, 125704 (2018).
- [7] S-Process manual, ver 2020.09 R, Synopsys, Inc, 2020.
- [8] S-Device manual, ver 2020.09 R, Synopsys, Inc, 2020.
- [9] P. Raha, J. W. Miller and E. Rosenbaum, "Time-dependent snapback in thin-film SOI MOSFET's," in *IEEE Electron Device Letters*, vol. 18, no. 11, pp. 509-511, Nov. 1997, doi: 10.1109/55.641428
- [10] H. Zhu, *et al.*, "The characterization of the built-in bipolar junction transistor in H-gate PD-SOI NMOS", *Solid-State Electronics*, **175**, 2021, <https://doi.org/10.1016/j.sse.2020.107919>.
- [11] S-Visual manual, ver 2020.09 R, Synopsys, Inc, 2020.